Robust and stretchable polymer semiconducting networks: from film microstructure to macroscopic device performance

Guoyan Zhang[†], Savannah Lee[†], Elizabeth Gutiérrez-Meza[‡], Carolyn Buckley[‡], Michael McBride[†], David A. Valverde-Chávez[‡], Yo-Han Kwon[†], Victoria Savikhin[⊥], Hao Xiong[†, ※], Tim J. Dunn[⊥], Michael F. Toney[⊥], Zhibo Yuan[‡], Carlos Silva[‡, +], Elsa Reichmanis[†, ‡, ◊]*

[†] School of Chemical and Biomolecular Engineering, Georgia Institute of Technology, 311 Ferst Drive NW, Atlanta, GA 30332 USA

[‡] School of Chemistry and Biochemistry, Georgia Institute of Technology, 901 Atlantic Dr, Atlanta, GA 30332 USA

[◊] School of Material Science and Engineering, Georgia Institute of Technology, 771 Ferst Dr NW, Atlanta, GA 30332 USA

[+] School of Physics, Georgia Institute of Technology, 837 State St NW, Atlanta, GA 30332 USA

[⊥] Stanford Synchrotron Radiation Light source Menlo Park, CA 94025, USA.

[※]College of Materials Science and Engineering, Donghua University, Shanghai 201620, P. R. China

Abstract: Although stretchable polymer-based devices with promising electrical performance have been produced through the polymer blend strategy, the interplay between the blend film microstructure and macroscopic device performance under deformation has yet to be unambiguously articulated. Here, we discuss the formation of robust semiconducting networks in blended films through a thermodynamic perspective. Thermodynamic behavior along with the linear absorption and photoluminescence measurements predict the competiton between polymer phase separation and semiconductor crystallization processes during film formation. Semiconducting films comprised of different pi-conjugated semiconductors were prepared and shown to have similar mechanical and electronic properties to films comprised of a model P3HT and PDMS blend. These results suggest that a film's microstructure and therefore robustness can be refined by controlling the phase separation and crystallization behavior during film solidification. Fine-tuning a film's electrical, mechanical, and optical properties during fabrication will allow for an advanced next-generation of optoelectronic devices.

1. Introduction

High-performance, robust polymer semiconductor-based devices, particularly those that are stretchable, rely on materials with both high charge carrier transport and excellent mechanical compliance. Current state-of-the-art research results suggest that charge transport and mechanical flexibility are mutually exclusive properties, and both are highly variable and sensitive to changes in the thin-film microstructure 1-3. While stretchable polymer-based devices with promising electrical and mechanical performance characteristics have been reported in semiconductor-insulator blends through a "nanoconfinement"effect or optimization of the active layer microstructure 4-8, the interplay between phase induced crystalline microstructure and development of effective charge transport pathways in conjugated polymers with/without strain has yet to be unambiguously articulated.

We recently suggested that high mechanical-electronic device performance could be achieved in stretchable devices through development of a continuous interpenetrating nanofibrillar semiconducting polymer network 9. It was found that both the mechanical and electronic properties began to exhibit enhanced performance when the weight fraction of semiconductor ($f_{semi.}$, wt%) was decreased to below 1 wt% in the semiconductor-insulator system. The results suggested that a practical strategy to build stretchable devices having robust active layers could be designed through control of semiconductor-insulator blend phase behavior. Polymer phase separation has been the subject of intensive studies as far back as the 1980s due to its role in the development of polymer microstructure and associated materials characteristics, including but not limited to electronic and mechanical properties 10-11. However, studies related to the evolution of conjugated polymer structure within an insulating polymer matrix/host, especially with ultra-low proportions of conjugated polymer (below 1 wt %), are scarce.

Here, we explore the evolution of thin-film microstructure in a highly stretchable bi-component polymer semiconducting film from a thermodynamic perspective, and evaluate the interplay between microstructure and semiconductor mechanical/electronic properties. Specifically, the ternary phase diagram of a semiconductor-poly(dimethylsiloxane)-chloroform system helped illustrate how diverse microstructures can be accessed from competing interactions associated with phase separation and crystallization processes. Linear absorption and photoluminescence measurements as a function of blend composition provided insight into the nature of two-dimensional excitons in these samples, providing further insight into the relationship between electronic/optical properties and solid-state microstructure.

Experimental evidence via film morphology and Grazing-incidence Wide-Angle X-ray Scattering (GIWAXS) suggest that a bridged semiconductor crystalline structure with either short range or long range order as well as low $f_{semi.}$ (0.5 wt %) will sustain efficient charge transport in addition to maintaining robust mechanical-electronic performance. In addition, the viability of the blend approach for the fabrication of robust semiconducting films and fully stretchable transistors was demonstrated by using a device array to drive commercial light emitting diodes (LEDs).

2. Results

2.1 Stretchable polymer semiconducting films. Stretchable, bi-component polymeric semiconducting films were prepared by blending different weight ratios of the conjugated polymer with polydimethylsiloxane (PDMS; Sylgard in a 10:1 weight ratio). Bi-component film charge transport characteristics were evaluated by fabrication of transistor devices using a bottom-gate/bottom-contact device configuration. The active layer films were deposited by spin-coating under ambient conditions, followed by annealing at moderate temperature under optimized processing conditions (see Methods, Supporting Information).

Taking poly(3-hexylthiophene) (P3HT)-PDMS semiconducting films as an example, the transistor parameters (charge carrier mobility (μ) and threshold voltage (V_{th})) of the blends, extracted from their transfer curves (Figure S1 and Table S1, see Supporting Information), are summarized in Figure 1a. Transistor performance was dependent on the proportion of P3HT (f_{P3HT}) in the blend, and could be divided into three distinct regimes. For blends with high f_{P3HT} (20 wt % - 100 wt %), semiconductor mobility remained essentially unchanged and was approximately the same as a 'pure' P3HT film. Surprisingly, blends of low f_{P3HT} (0.35 wt % - 20 wt %) with PDMS exhibited higher mobility. In particular, the charge transport characteristics of f_{P3HT} (below 1 wt %, optimized result is about 0.5 wt %. *Note that, in the following discussion, we used 0.5 wt% as the optimized ratio instead of 0.49 wt% to make the comparasion with other blending ratios.*) were significantly enhanced, whereby the mobility was about ten-fold higher than the P3HT control films. For trace f_{P3HT} (0.2 wt % - 0.3 wt %) active layer, the mobility decreased, perhaps because of the proportion of P3HT was near or perhaps below the vicinity of the percolation threshold (about 0.17 wt %) and thus the density of effective charge transport pathways between the electrodes was reduced. Note that, compared to the blend films at 100-95 wt%, others displayed lower V_{th}, the large difference is mainly because of the different thickness of the protective PDMS layer in the blended films (Figure S2, see Supporting Information). The thinness of the film will likely result in a very thin PDMS layer on top of the P3HT layer, which cannot fully protect the P3HT component in air during the film formation and device fabrication process. Notably, similar transistor performance was observed for other semiconducting polymers: poly[2,5-(2-octyldodecyl)-3,6-diketopyrrolopyrrole-alt-5,5-(2,5-di(thien-2-yl)thieno [3,2-b]thiophene)] (DPP-DTT)-PDMS (Figure 1c and Figure S3a, see Supporting Information) and poly(2,5-bis(2-octyldodecyl)3,6-di(pyridin-2-yl)-pyrrolo[3,4-c]pyrrole-1,4(2H,5H)-dionealt-2,2′-bithiophene) (DPPDPyBT)-PDMS (Figure 1d and Figure S3b, see Supporting Information).

The elasticity of these semiconducting films was investigated using both thin semiconducting films fabricated on a soft elastic substrate (Ecoflex 0010 with elongation of break at 275%) and for comparison to our previous studies, thick, free standing films 9. In the case of the thin-films, the semiconducting blends were deposited on soft elastic substrates, stretched to a certain strain and then unloaded, to observe the on-set strain of wrinkle formation; freestanding thick films were characterized using an Instron 5567 instrument to collect the strain-stress curves. To observe the dependence of elasticity on blend composition, three representative P3HT-PDMS ratios were evaluated. Specifically, samples with f_{P3HT} equal to 80 wt %, 15 wt %, 0.5 wt % were selected

(Figure 1b, and Figure S4, see Supporting Information). Surprisingly, optimized 0.5 wt % P3HT-PDMS semiconducting films exhibited improved stretchability relative to other blend ratio samples. The enhanced mechanical properties may derive from the microstructure adopted by the semiconducting polymer in the insulating polymer matrix, warranting further investigation.

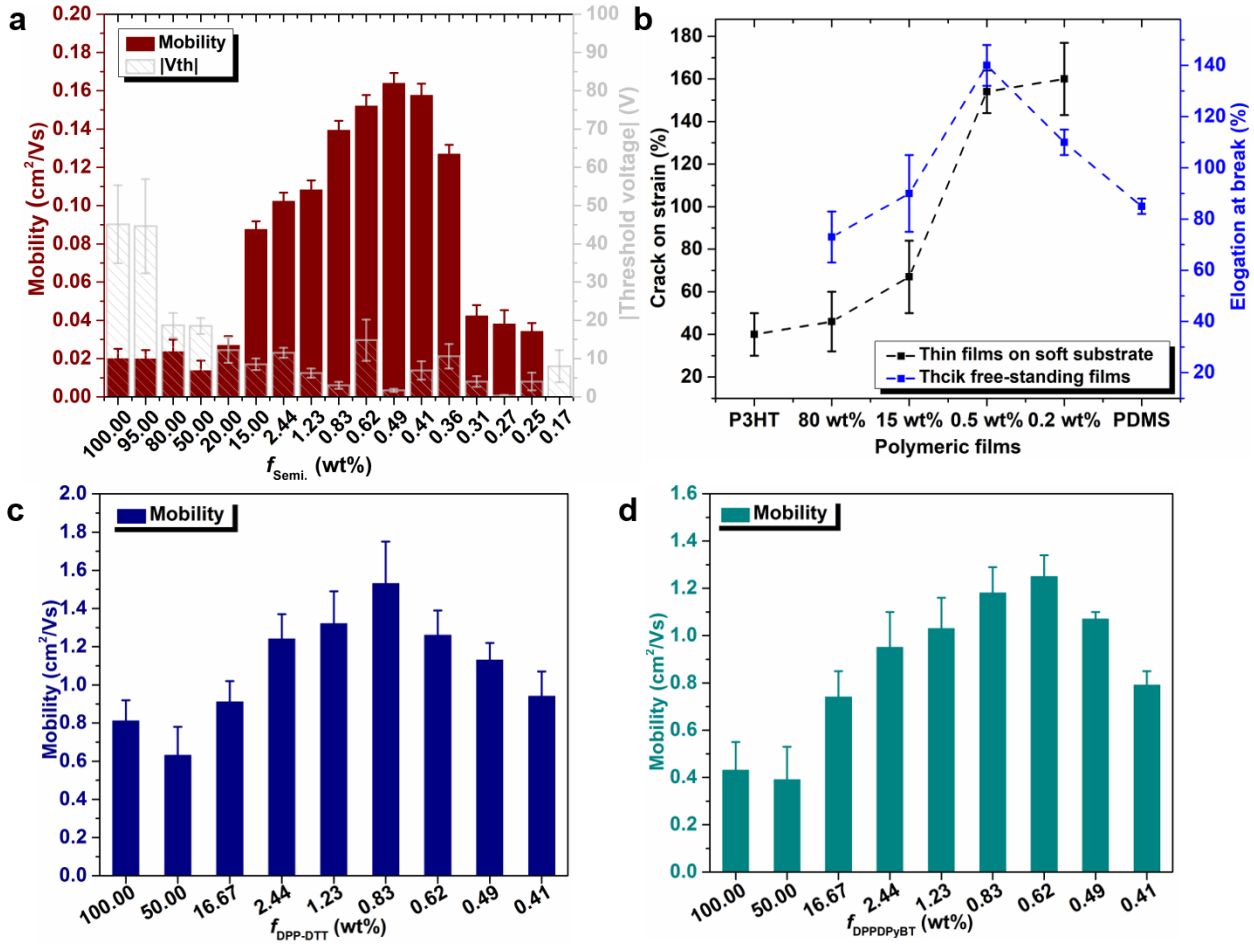

Figure 1. **The effect of the $f_{semi.}$ in the active layer on the transistor performance.** Blend film OFET characteristics where the blends have different f_{P3HT} (a). (b): Crack and elogation at break of selected f_{P3HT} (80 wt %, 15 wt %, 0.5 wt %) films. Semiconducting films comprised of different pi-conjugated semiconductors and their OFETs characteristics: $f_{DPP\text{-}DTT}$ (c), $f_{DPPDPyBT}$ (d).

2.2 Semiconductor-PDMS Phase Behavior. The final blend microstructure evolves during a dynamic process as solvent evaporates from the solidifying film. To interrogate that process from a fundamental perspective, a ternary phase diagram was constructed to evaluate interactions between the three components, their mixing behavior and the ultimate thin-film morphology 12-14. The f_{P3HT} values used for this study were selected to be the same as those used to evaluate mechanical performance.

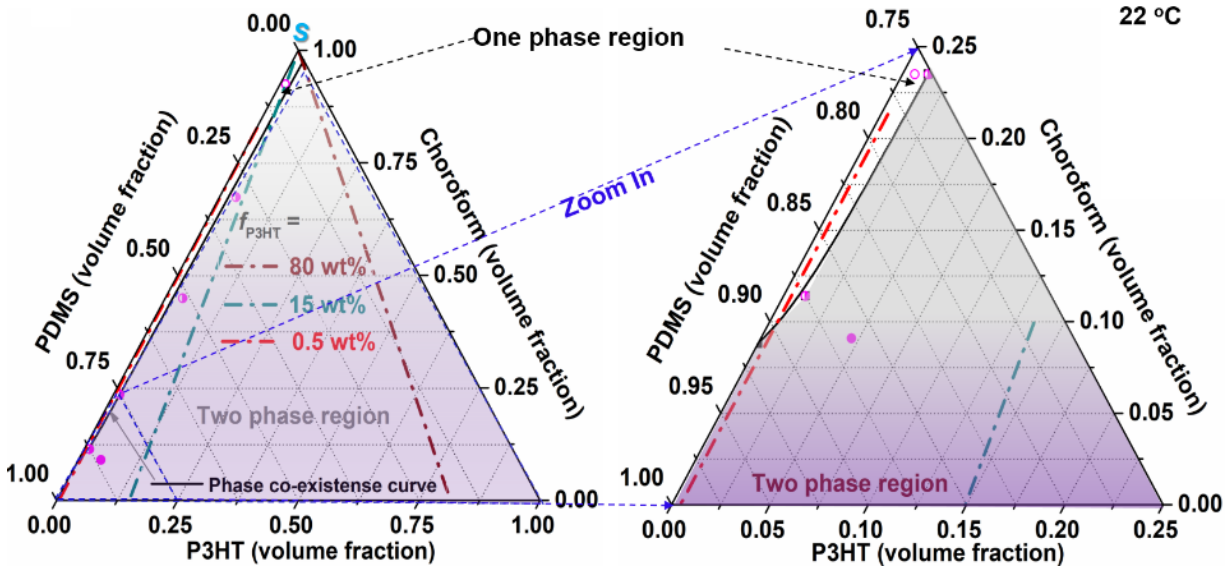

Figure 2. **Ternary phase diagram of the $CHCl_3$-PDMS-P3HT blend, calculated using Flory–Huggins theory**. Volume fractions of the three components are indicated on the axes. Data was obtained from cloud-point determination by laser-light scattering and optical microscope examination of various starting compositions of the blend solutions as the solvent, $CHCl_3$ evaporated over several days. Open symbols: transparent one-phase system; solid symbols: cloudy two-phase region. The black line represents the binodal compositions; the dot-dashed lines indicate the change in blend composition upon solvent evaporation for f_{P3HT}: 80 wt% (wine), 15 wt% (cyan) and 0.5 wt% (red), from right to left. "***s***" means the starting solution state.

Figure 2 depicts the thermodynamic phase diagram for $CHCl_3$-P3HT-PDMS, which presents with a substantial immiscibility region. The black solid line and the colored dot-dashed lines indicate the co-existence curve and the different blend ratios, respectively, as calculated from Flory-Huggins theory 14. It was previously demonstrated that $CHCl_3$ is a better solvent for PDMS (> 500 mg/mL in $CHCl_3$) than P3HT (< 25 mg/mL in $CHCl_3$), that P3HT has a higher surface energy than PDMS (19.3 mJ/m^2 vs. 7.3 mJ/m^2), and that the interaction parameter, $\chi_{PDMS/P3HT}$, between the two polymers is large (0.55) 9. These results point to a highly skewed, difficult to discern miscibility region for $CHCl_3$-P3HT rich compositions on the scale of the diagram, and thus phase separation is highly likely during solvent evaporation. In the present three-component case, the initial mixture is solvent rich and exists as a single phase; during spin coating, the solvent begins to evaporate and the ternary system passes through a phase separated binary fluid state ($CHCl_3$-PDMS and $CHCl_3$-P3HT) to eventually arrive at the final solvent-free PDMS-P3HT film. A complicating feature in the above mechanistic view is that the semiconducting component can simultaneously undergo processes such as self-assembly and crystallization. Thus to develop a comprehensive understanding of the process, the self-assembly and crystallization behavior of the semiconducting component during phase separation was also evaluated.

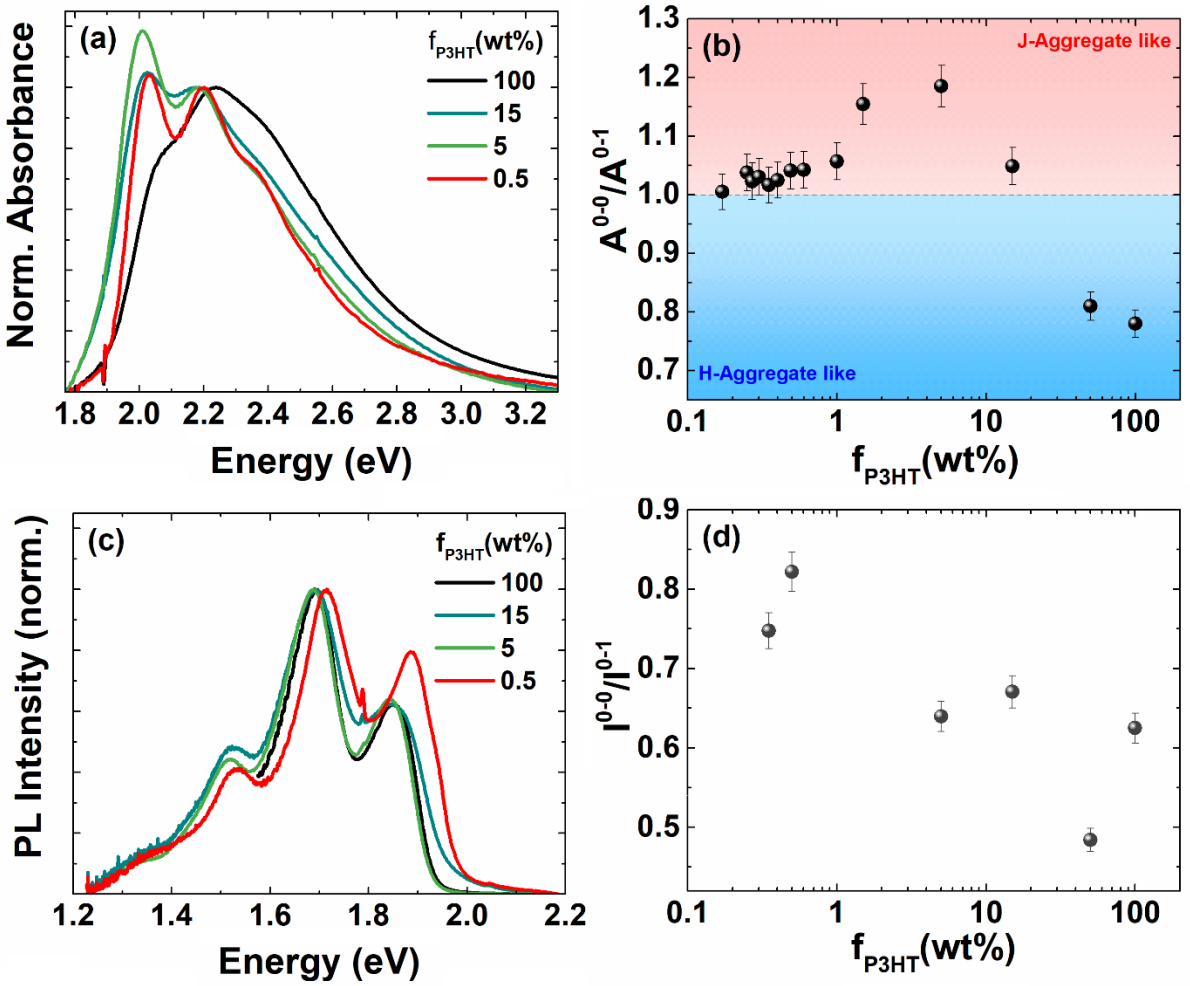

Figure 3. Absorption and photoluminescence spectra of P3HT: PDMS blends. (a) Absorption spectra at various fractions of P3HT, measured at room temperature (295K). (b) Ratio of the relative absorbance of the origin of the vibronic progression with respect to the 0-1 peak. (c) Photoluminescence spectra at corresponding fractions of P3HT, measured at 5 K. (d) Ratio of the relative absorbance of the origin of the vibronic progression relative to the 0-1 peak.

UV-vis and photoluminescence (PL) spectroscopy (additional data are shown in Supporting Information, see Figure S5, S6 and S7) provide valuable insight into the organization of conjugated polymers into aligned aggregates and/or crystalline species 15-17. UV-vis analysis suggested that for f_{P3HT} (0.5 wt %), conjugated polymer aggregation was initiated in the liquid state and was further developed in the dry, solidified film. (Figure S5 and Figure S6, see Supporting Information) For this low f_{P3HT} sample, the aggregate fraction, as calculated from Franck-Condon fits to the absorption spectra was estimated to be 30 % 18; while during the solvent evaporation process, the film experienced a wet, solid film state, finally achieving a dry, solid state having an increased proportion of aggregates (71 %). For other f_{P3HT} (50 wt %, 15 wt %) blends, the aggregate fraction was estimated to be below 3 % in the liquid state, and 61.12 % (50 wt %), 62.86 % (15 wt %) for the dry solidified films. These results suggest that when the proportion of P3HT in solution is low, below about 1.5 %, the conjugated polymer begins to self-assemble to form aggregates while still

in the liquid state. Alternatively, for the high f_{P3HT} samples, aggregation was not observed until the evolving film entered the wet solid state.

The absorption and photoluminescence spectral lineshapes as a function of blend composition provide further insight into the nature of the two-dimensional exciton, which yields complementary information to structural and electrical characterization since they are sensitive to interactions on molecular lengthscales. Figure 3(a) displays the absorption spectra of various blends with fraction of P3HT indicated in the legend. We observe that the ratio of absorbance of the vibronic origin (0-0) to 0-1 depends on composition. This dependence is displayed systematically in Figure 3(b). In semicrystalline polymeric materials such as P3HT, excitons are successfully modelled within a hybrid photophysical aggregate model in a weak coupling limit in which both intermolecular (H-like) and intramolecular (J-like) excitonic coupling competes to establish the two-dimensional exciton spatial coherence function, which describes the spatial extent of the exciton 19-21. The effect of the exciton coherence is encoded on the 0-0 absorbance with respect to the rest of the vibronic progression. When intermolecular coupling is dominant (H-like aggregate), the 0-0 absorbance is suppressed with respect to the rest of the progression. On the other hand, when intrachain coupling dominates (J-like aggregate), the 0-0 absorbance is enhanced. An isolated polymer chain, not part of a photophysical aggregate, would have approximately equal intensity of 0-0 and 0-1 peaks if the Huang-Rhys parameter is 1, which is typically the case in polymers such as P3HT 22. Figure 3(b) demonstrates that in most blends, the P3HT aggregates are predominantly J-like, in which intramolecular excitonic coupling is dominant with respect to the intermolecular coupling. Only in the cases of f_{P3HT} = 50 and 100% is the aggregate dominantly H-like in the sample set displayed in Figure 3(b). This corresponds to a low mobility regime in Figure 2. We note that dominantly J-aggregate behavior, reflected by the absorption lineshape, is observed in blends of conjugated polymers with insulating polymers 23 or when processing in solvent mixtures of polar and apolar solvents 24, 25. Increased J-like character in P3HT aggregates is typically associated with increased intrachain planarity due to decreased torsional disorder within the chain 20. We observe a peak of the 0-0/0-1 absorbance ratio at $f_{P3HT} \sim 5\%$, suggesting that this blend ratio features the highest degree of intrachain coupling, likely associated with intrachain torsional order. The range of the absorbance peak ratio > 1 is maximum over the range of highest mobility as reported in Figure 2.

In contrast to the absorption lineshape, the PL lineshape contains additional information on the nature of the disordered energy landscape that the exciton experiences. As in the absorption spectrum, the 0-0 PL intensity is suppressed in a H aggregate but enhanced in a J aggregate. The PL spectra displayed in Figure 3(c) all reveal $I_{0\text{-}0} < I_{0\text{-}1}$, suggesting predominantly H-like aggregate behavior of the emitting state for all blend compositions, where interchain excitonic coupling is dominant. For a H aggregate, the 0-0 PL intensity is strictly zero in the absence of energetic disorder due to symmetry. However, energetic disorder breaks symmetry and 0-0 intensity is increasingly recovered as the disorder width increases. However, if the disorder is highly correlated, meaning that the energy of a particular chain in an aggregate persists over distances that are long compared to the interchain separation, then the symmetry-breaking effects of disorder

are suppressed, and the 0-0 intensity decreases in spite of the energetic disorder width 20, 26. In Figure 3(d), we observe that the 0-0/0-1 PL intensity ratio decreases systematically as f_{P3HT} increases. Assuming that the interchain excitonic coupling strength and the total energetic disorder width varies weakly over this trend, then the energetic landscape appears more highly correlated as f_{P3HT} increases. Comparison with the absorption lineshape in Figure 3(a) shows that the interchain excitonic coupling only dominates at the highest P3HT compositions, suggesting that the effect of spatial correlation of the energetic disorder is the dominant effect in the trend in Figure 3(d). This suggests that as the P3HT fraction increases, the energy of adjacent chains in an aggregate is more highly correlated. Although the energy of one aggregate might vary with respect to another one, the energy of constituent chains is more highly correlated with higher fraction of P3HT.

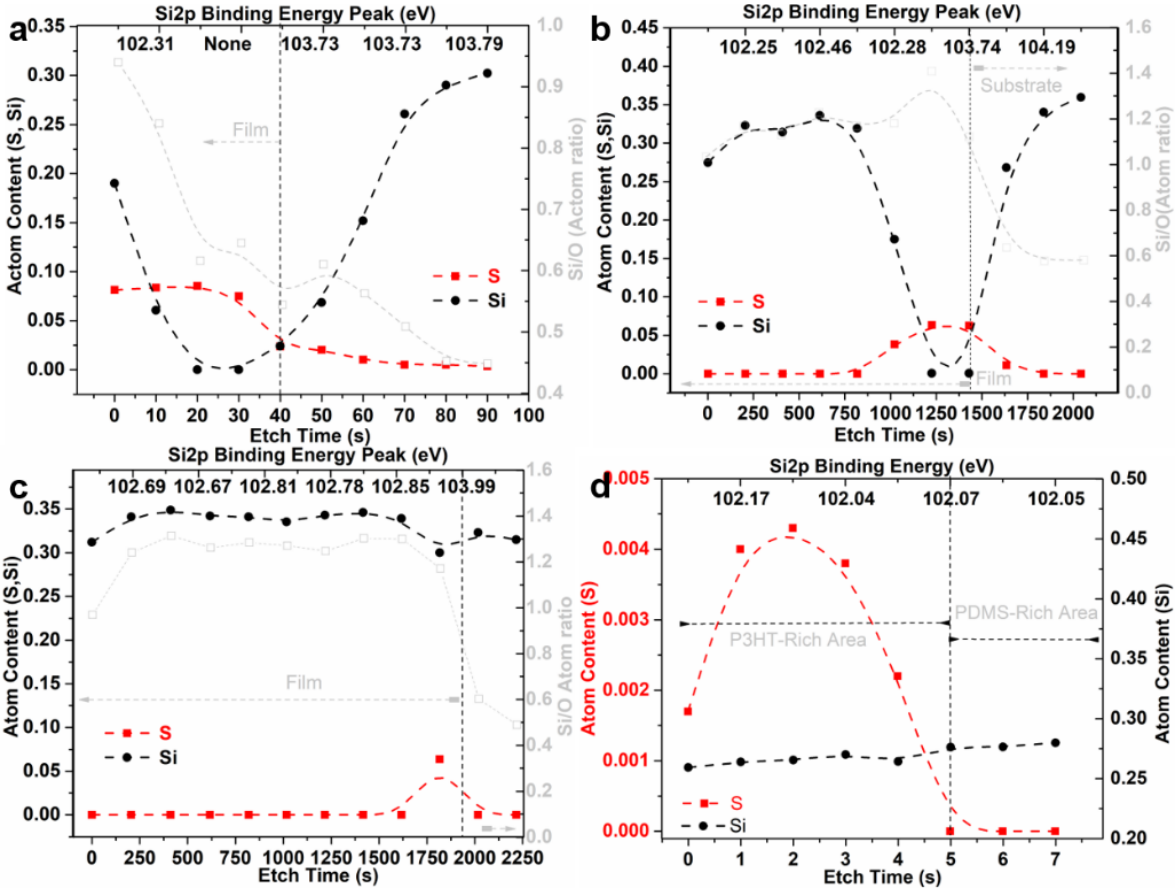

Figure 4. **XPS etching depth profile of the blend films show elements distribution along the etching direction.** (a): For 80 wt %, etching direction: from top to bottom. (b): For 15 wt %, etching direction: from top to bottom. (c): For 0.5 wt %, etching direction: from top to bottom. (d): For 0.5 wt %, etching direction: from bottom to top. Four different points were selected to collect the depth profiles for each sample.

Information regarding the composition profiles of the solidified conjugated polymer-PDMS films was derived from atomic force microscopy (AFM) and X-ray photoelectron spectroscopy (XPS). Using P3HT-PDMS as an example, AFM was used to interrogate the air and substrate interface

morphologies of the semiconducting films comprising 80 wt %, 15 wt % and 0.5 wt % P3HT (Figure S8, see Supporting Information). Fibrillar crosshatched features appeared at the bottom, substrate interface of f_{P3HT} (0.5 wt %), while the air interface of the same sample presents a featureless, amorphous-like morphology similar to that observed for pure PDMS films. Increasing the proportion of P3HT to 15 wt % led to the appearance of cluster-like features at the substrate interface; and for 80 wt % semiconducting polymer, both surfaces exhibited similar cluster-like structures.

Depth-dependent XPS measurements using sulfur (S, solely present in P3HT) and silicon (Si, solely present in PDMS) facilitated evaluation of the polymer distribution in the film, as shown in Figure 4. The Si to O ratio and Si binding energy (BE, eV) were used to differentiate Si originating from PDMS (Si-1; BE: ~102 -103 eV, Si: O = 1:1) from that associated with the substrate (Si-2; BE: ~104 eV, Si: O = 1:2) (Figure S9, see Supporting Information). When the blend composition was predominately conjugated polymer, i.e., f_{P3HT} (80 wt %, Figure 4a), S was detected throughout the thickness of the film, while Si-1 was strictly detected at the air interface. For f_{P3HT} (15 wt %, Figure 4b), the substrate interface appeared to be predominately P3HT as evidenced by the presence of a S signal with no apparent Si-1, while the air interface region was Si-1 rich. Both elements were detected in the middle, 'bulk' area of the film that was adjacent to the substrate.

Accurate analysis of the elemental distribution in low f_{P3HT} films required etching into the film from both the air (Figure 4c) and substrate interfaces (Figure 4d). For f_{P3HT} (0.5 wt %), Si-1 was readily discerned throughout the entire thickness of the film; while S was limited to the region directly adjacent to the substrate. In addition, four different points on the same film were interrogated, revealing that S was not uniformly present throughout the substrate interface region. In other words, S was absent in some of the etching positions for f_{P3HT} (0.5 wt %), suggesting the presence of a "*birds-nest netted structure*" for the bottom P3HT layer at the substrate interface. The XPS results are reminiscent of the lateral/vertical micrometer scale phase separation frequently found upon mixing two limited miscibility polymers 27.

The combined spectroscopic and microscopic results presented above provide insight into the organization and crystallization of conjugated polymers within insulating matrices. The phase separation behavior for different blend ratio films is presented in Figure S10 in the Supporting Information. Specifically, at high f_{P3HT} (80 wt %), PDMS appears to be distributed laterally within a P3HT matrix; as the f_{P3HT} decreased to a point where the conjugated polymer became the minor component, i.e., f_{P3HT} (15 wt %), the structure became more complex whereby "*two distinct layers*" were observed, namely a PDMS-rich top layer at the air interface and P3HT-rich layer at the substrate interface. This structure suggests that the polymer components undergo vertical phase separation, which is often found in polymer blends 28-32. Upon decreasing f_{P3HT} to an ultra-low level (0.5 wt %), further complicates the phase behavior. Conceivably, when the proportion of conjugated polymer is less than 1 wt %, the final continuous reticulated nano-fibrillar structure, where the gaps between the conjugated polymer networks become filled with PDMS, represents a synergy between P3HT crystallization and the solidification of amorphous insulating material.

The ternary phase diagram (*vide supra*) provides support for the supposition that low f_{P3HT} (0.5 wt %) favors formation of a fibrillar semicrystalline conjugated polymer network, while higher f_{P3HT} (80 wt %, 15 wt %) tends to form a structure that is heterogeneous with both amorphous and semicrystalline regions. First, examination of the solvent content from the start point "***s***" to the liquid two-phase boundary (*black solid line*) as a function of f_{P3HT} (Figure 2) demonstrates that solvent remains in the system for a longer period of time for f_{P3HT} (0.5 wt %) vs. f_{P3HT} (80 wt %, 15 wt %). This phenomenon provides for a prolonged time-frame for liquid-liquid phase separation to take place in f_{P3HT} (0.5 wt %). For the higher weight fraction semiconductor blends, 80 wt % (*wine dot-dashed line*) and 15 wt % (*cyan dot-dashed line*) blend, only 6.3 vol % and 12.5 vol % of solvent, respectively must evaporate for the samples to reach to liquid two phase boundary. Notably, for f_{P3HT} (0.5 wt %, *red dot-dashed line*), that boundary is reached only when 87.5 vol % of the solvent is evaporated from the system. As a result, the f_{P3HT} (0.5 wt %) blend system remains homogeneous and solubilized for a longer period of time, which favors continuous growth of the semiconducting fibrils, along with nucleation and growth of remaining 'amorphous' P3HT. Given the presence of additional solvent/solvent vapor, longer fibrillar structures can form in the ultra-low conjugated polymer samples vs. higher, 80 wt % and 15 wt % blends. In other words, P3HT crystallization behavior is predominant in the f_{P3HT} (0.5 wt %) early phase separation process. The final continuous crystalline, fibrillar reticulated structures result from the competition between semicrystalline nucleation and curing-induced cross-linking of the PDMS matrix in the final blend film solidification process.

2.3 Interplay between microstructure and robust charge transport pathways. The mechanical-electrical performance of bi-component active layers with different microstructures were evaluated through a delamination-stretching-relamination process. More than twenty devices were fabricated and characterized from each composition and different strain (0 %, 100 %, and release to 0 %). Considering the different initial mobility due to different semiconductor content, the normalized average mobility μ/μ_0 was plotted as a function of strain to determine electrical performance (Figure 6a). Unexpectedly, the value of μ/μ_0 only slightly decreased for f_{P3HT} (0.5 wt %) transistors when subjected to 100 % strain; after release of strain, they recovered to close to their original value, a result that was consistent with previous results and distinctly different from the performance of higher weight fraction samples. More interesting, when strain was released and the film returned to its original state, low f_{P3HT} exhibited better electrical recovery than the high f_{P3HT} counterparts ($R = \mu_r/\mu_0$, μ_r: mobility of release strain, μ_0: mobility of fresh film): $R_{0.5}$ (93.34%) > R_{15} (59.42%) > R_{80} (21.35%) > R_{100} (4.61%).

In light of the results presented above, f_{P3HT} (0.5 wt %) films were evaluated further in order to examine their stretching stability and reliability. Notably, after 1000 stretching cycles, μ/μ_0 underwent almost no change and the devices exhibited reliable operation, as presented in Figure 6b. The representative transfer curves of the bi-component and neat P3HT films under different strain are provided in Figure 6c.

Similar phenomena were observed in blends of DPP-DTT-PDMS (Figure 6d) and DPPDPyBT-PDMS (Figure 6e). Degraded mobility of all neat polymer thin-film transistors was evident when the devices were subjected to 100 % strain. Optimized charge transport performance was obtained in transistors comprised of bi-component active layers with low semiconductor composition: $f_{\text{DPP-DTT}}$ (0.8 wt %) and f_{DPPDPyBT} (0.6 wt %). Moreover, the mobility of these optimized bi-component film transistors was over 1.0 $cm^2/V{\cdot}s$ under 100 % deformation, which exceeded their neat counterparts by six to eight fold. OFET transfer curves did not change significantly with respect to the unstrained state after multiple stretching cycles and electrical performance appeared stable (Figure S11, see Supporting Information). The results demonstrate that the phase behavior of multicomponent thiophene-based semiconducting polymer – insulating polymer blends can be manipulated to afford well-aligned networks with effective charge transport pathways at low concentrations of the active material. Presumably, the apparent exceptional electrical-mechanical performance derives from the competitive interactions induced by film micromorphology.

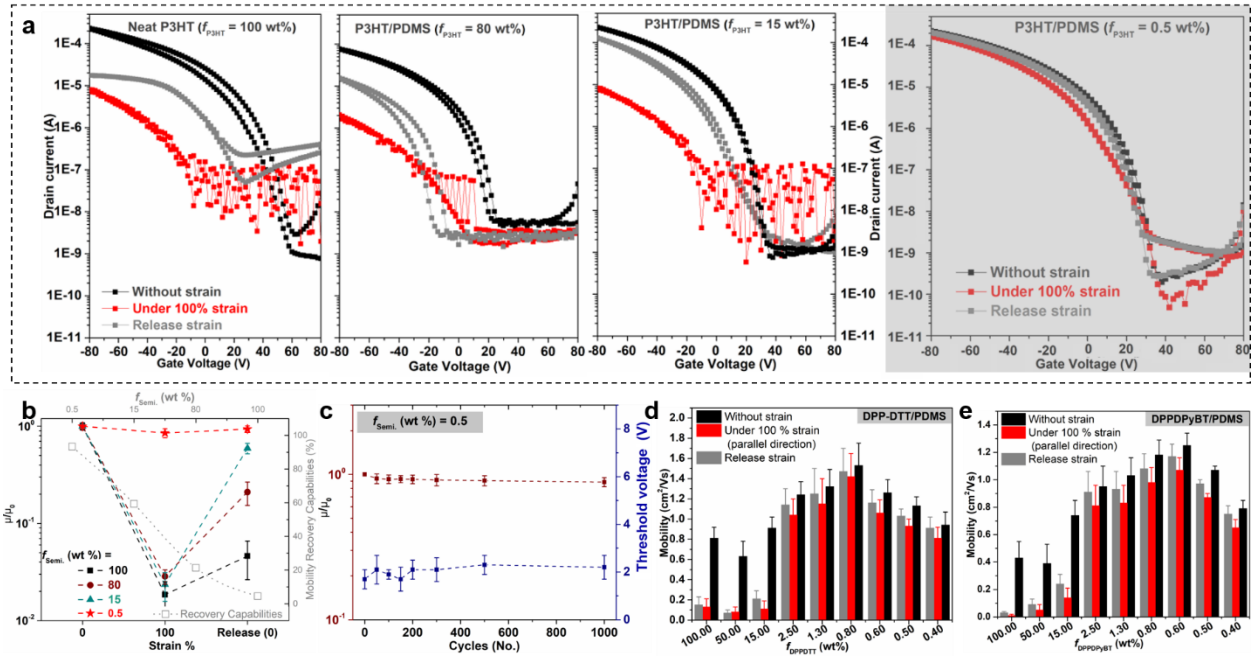

Figure 6. Effect of the $f_{\text{semi.}}$ on the transistor mechanical-electrical performance. (a): The original OFET transfer curves (V_D = - 80 V) of the transistors with four distinct f_{P3HT} (100 wt %, 80 wt %, 15 wt %, 0.5 wt %) under different strain state. *Note that*: The original OFET transfer curves of f_{P3HT} (0.5 wt %, with gray shading) is consistent with previous results 9. (b): Normalized mobility performance of films with 100 wt % (neat film), 80 wt %, 15 wt % and 0.5 wt % of P3HT under different film strain conditions. μ_0 denotes the original mobility. (c): The mobility stability of the OFETs with optimized semiconducting films (0.5 wt %) after different stretching cycles. (d, e): Similar mechanical-electrical phenomena in DPP-DTT-PDMS and DPPDPyBT-PDMS semiconducting blend films.

The viability of the blend approach that uses low proportions of conjugated polymer (~ 1 wt%) for the fabrication of robust, transparent semiconducting films and fully stretchable transistors, was demonstrated previously 9. Here, the effectiveness of an active layer based upon a conjugated polymer-insulating polymer blend is further demonstrated through fabrication of a stretchable transistor array that serves as the drive electronics for light-emitting diodes (LED) \(Video S1, See Supporting Information).

The morphologies of the films when subjected to strain, as well as their release state were also characterized by AFM (Figure S12, see Supporting Information). The semicrystalline-fibrillar networks in f_{P3HT} (0.5 wt %) appeared to stretch largely in the direction of applied strain. Interestingly, the fibrils exhibit continuous and greater length in the PDMS matrix at 100 % strain. After release of strain, the fibrillar network structure returned to the unstrained, seemingly loose network status with no observed signs of cracking. After 1000 stretch-release cycles, the continuous networks were clearly apparent, with negligible changes. In contrast, the f_{P3HT} (80 wt %) films were seriously damaged under 100 % strain, and film roughness increased considerably vs the initial state (Figure S13, see Supporting Information). Although the f_{P3HT} (15 wt %) films suffered some damage under strain, the semiconducting network appeared to retain its primary structure and original roughness upon release of stain. The results are consistent with an apparent correlation between blend morphology from the nano to macro-scales and respective electrical-mechanical performance.

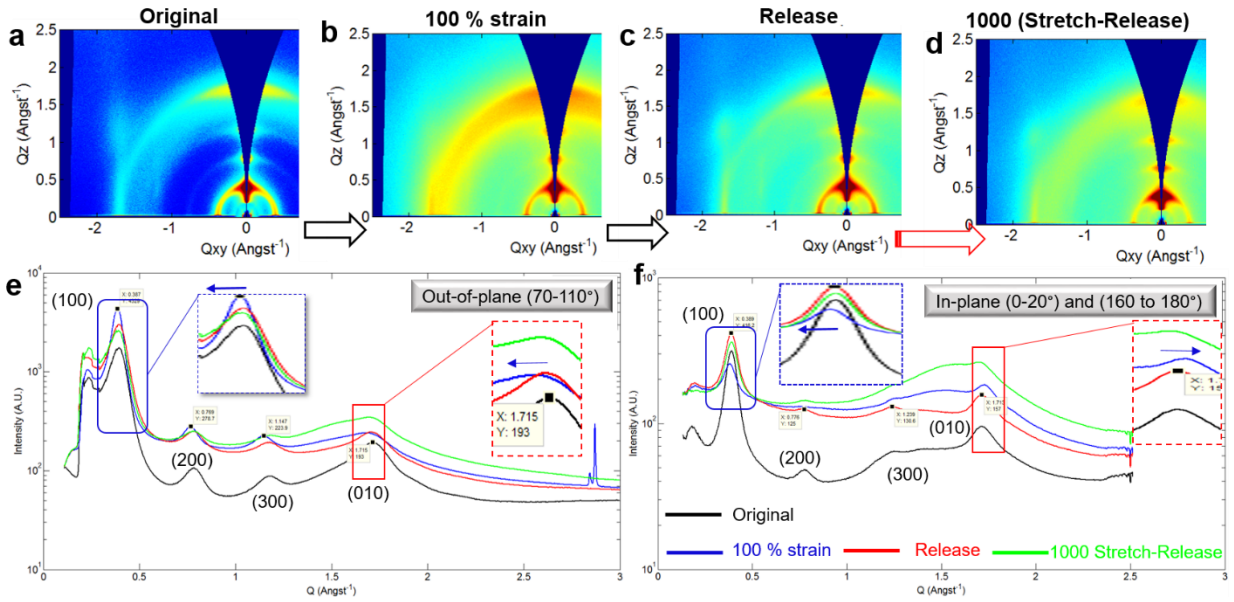

Figure 7. Crystalline orientation changes in the strained semiconducting films. 2D-GIWAXS maps (a-d) and 1D-scattering profiles (e, f) films under different state: a: original, b: strain 100 %, c: release strain, d: after 1000 stretch-release cycles.

Since the orientation of the crystalline nanofibrillar structure in the bi-component films during the stretch-release cycles are a critical element to their mechanical-electrical performance, f_{P3HT} (0.5

wt %) films were interrogated using grazing-incidence wide-angle X-ray scattering (GIWAXS) 33. **Figure 7** presents two-dimensional GIWAXS profiles and one-dimensional scattering profiles of the bi-component film under different conditions: unstrained, under 100 % strain, release to original state, and after 1000 strain-release cycles. For the unstrained film (black line), release to original state (red line), and after 1000 strain-release cycles (green line)), four diffusive elliptical-like patterns were observed along the out of plane direction at q_z (Å^{-1}) = 0.396, 0.792, 1.168, which are associated with a lamellar spacing of the (100) plane (2π/0.396 = 15.86 Å), (200) plane (2π/0.792 = 7.93 Å), (300) plane (2π/1.168 = 5.38 Å) and at q_z (Å^{-1}) = 1.715, corresponding to a π-π stacking distance in the (010) plane (2π/1.715 = 3.66 Å). The (010) peaks also appeared in the in plane directions (a similar d-spacing of 3.67 Å), suggesting a heterogeneous microstructure with a mix of edge-on and face-on orientations 33, 34. In addition, the (*h*00) diffractions show higher intensities out of plane, indicating that the conjugated lamellae were oriented preferentially in the plane of the film, which is favorable for charge transport in OFETs devices 33, 34. For the strained films, however, a "*blue shift*" was observed for the peak positions for the (*h*00) along both the q_z axis and $q_{x,y}$ axis (Table S2, see Supporting Information), indicative of an increase in d-spacing in the direction along the side chains. Interestingly, a "*red shift*" at the $q_{x,y}$ axis of the (010) position was found.

From a mechanistic perspective, we consider the P3HT semicrystalline packing to comprise "*columns of unit cells*" 35. When subjected to a stretch strain, the "*polymer semicrystalline unit cell*" in the lamellar stacking direction glides to create a dislocation; after release of strain, the "*dislocation metastable structures*" are able to slip back with the help of the elastic PDMS matrix (**Scheme 1**).

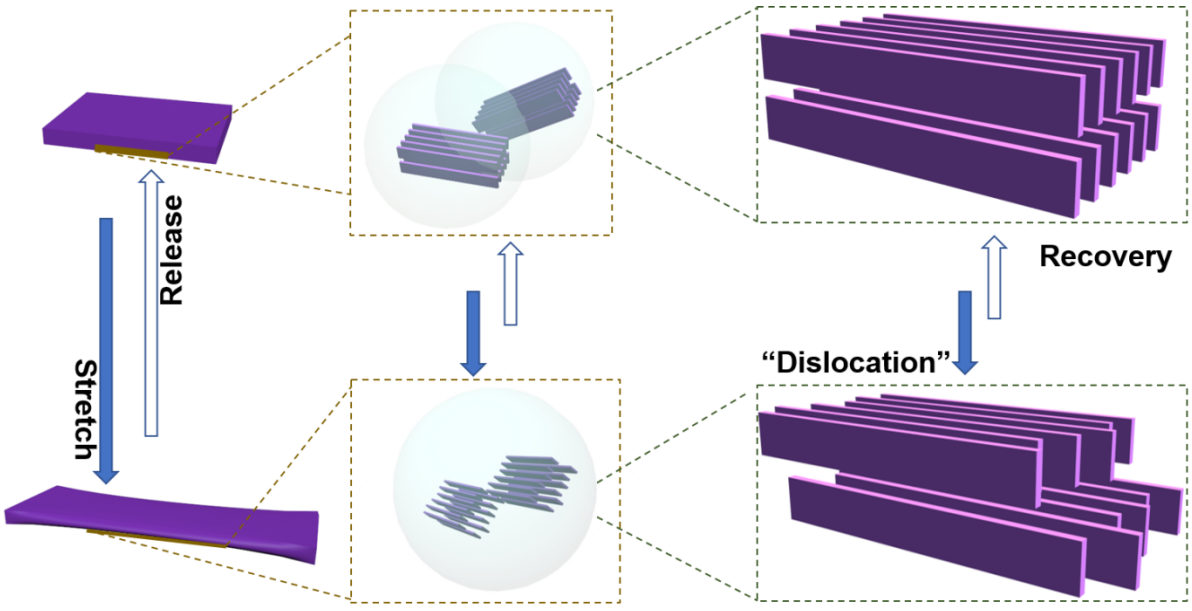

Scheme 1. The robust stacking structure of the P3HT in the blend f_{P3HT} (0.5 wt %) film.

2.4 Mechanistic requirements for robust, stretchable semiconducting networks. Based on the results presented above, **Scheme 2** and **Figure S10** in Supporting Information provide a mechanistic perspective on the development of robust semiconducting networks in conjugated polymer – insulating polymer blends. By taking advantage of competing processes, including phase separation, crystallization and thin-film solidification, a robust semicrystalline-fibrillar structure that retains effective charge transport pathways under strain was created**.**

More specifically, when the proportion of conjugated polymer in the starting liquid state is exceptionally low, on the order of 1.0 wt%, the semiconductor is in an amorphous state and is essentially surrounded by PDMS in the common solvent. Due to their dissimilar entropy, surface energy and solubility parameters, along with the different crystallization behavior, the presence of PDMS facilitates self-assembly and aggregation of amorphous conjugated polymer into short nanofibrillar structures (Figure S5, see Supporting Information). Upon deposition and subsequent spin coating, the solvent rapidly evaporates, whereby phase separation, rather than simple unfavorable interactions between the two polymer components, becomes dominant. When the fraction of conjugated polymer is high, favorable polymer-solvent interactions dominate the unfavorable polymer-polymer interactions, thereby inhibiting conjugated polymer aggregation 36.

During phase separation, interfacial instabilities in the transient wetting layers (air-polymer, insulating polymer-conjugated polymer and polymer-substrate) create an instantaneous "spinodal wave" 37. At this moment, the polymer chains are thermally unstable due to thermally driven molecular motion and dissimilar in surface free energy 38. In addition, the conformational entropy of the semiconductor chains will be lower for a thin integrated layer versus a thick layer. Thus, that the impact of the "spinodal wave effect" in conjunction with the thickness of the conjugated polymer layer on the aggregated semiconductor structure in a blend film will manifest when f_{semi} is sufficiently low (below 1 wt %).

Late in the phase separation process (i.e., the film solidification process) and after liquid-liquid phase separation, the short nanofibrillar structures serve as nucleation sites for the growth of long semicrystalline fibers (serves as long range charge transport pathway in transistors). Simultaneously, amorphous, solubilized conjugated polymer is also able to aggregate to form additional short semicrystalline fibers that segregate throughout the uncured PDMS layer lying adjacent to the conjugated polymer layer forming at the substrate interface. Finally when the dry solid film is formed, the semiconducting layer comprises a staggered network of crossed, short and long semicrystalline fibrils within the cured PDMS matrix. This heterogeneous microstructure possesses both long-range and short-range ordered regions that are interconnected by bridging polymer chains, which supports efficient charge carrier transport through the conjugated polymer network.

When subjected to strain, the long fibrillar aggregates that support efficient charge transport are effectively protected by the elastic matrix. The lamellar stacking (slow charge transport pathway) and the π-π stacking (fast charge transport pathway) distances of the "*polymer semicrystalline unit cell*" may change slightly because of the strain, but are expected to retain their order in the π-

stacking direction, slipping back to their original state with the help of the elastic matrix. Thus under strain, the long and short ordered fibrils comprising the heterogeneous microstructure are spatially sufficiently close to form an interconnected system, thereby retaining a semiconducting network that sustains efficient charge transport. This generalized mechanism explains the seemingly abnormal high mechanical-electrical performance in ultra-low semiconductor blend films reported previously 9, and suggests that control of phase separation in multicomponent blend is a valuable strategy to access robust polymer materials for future generations of organic electronic devices.

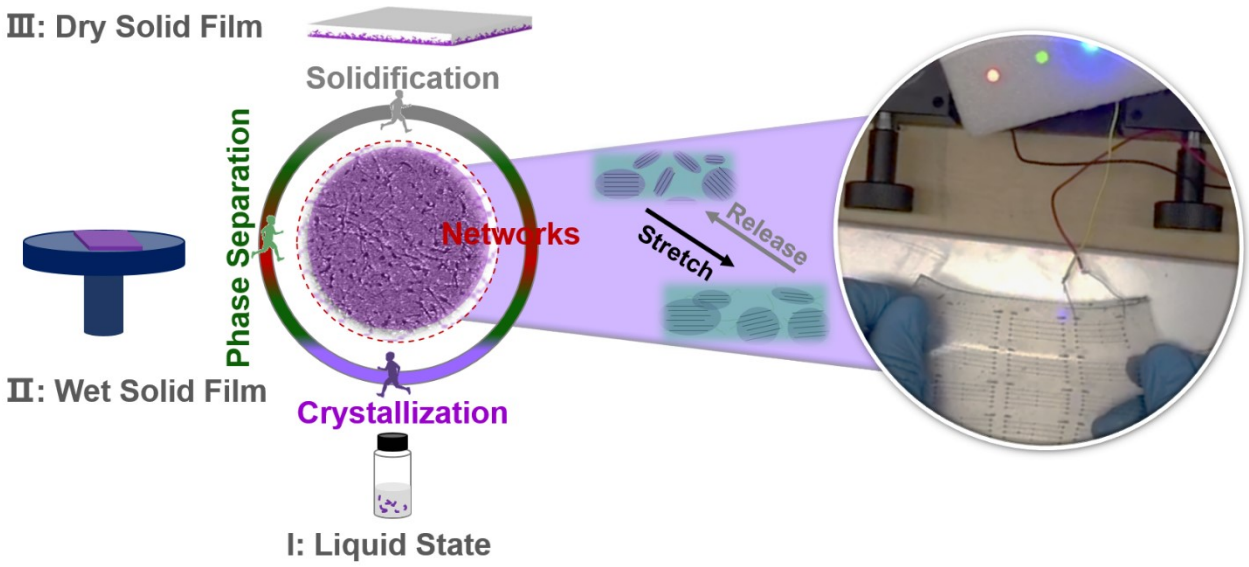

Scheme 2. Competition induced semiconducting network formation for robust and stretchable polymeric electronic devices.

3. Conclusions

The mechanism associated with the evolution of efficient charge transport pathways in semiconducting/insulating polymer blends deposited from solution was systematically investigated. Further, the interplay between thin-film microstructure and macroscale electronic performance in a transistor configuration with/without strain was interrogated. The results demonstrate that through control of competing processes, including phase separation, semiconductor crystallization and amorphous insulating polymer cure, robust, interconnected semiconducting networks can be created. The development of such robust networks in evolving solidified films during the deposition process is imperative for construction of efficient charge transport pathways. Notably, use of an elastic insulating component as the matrix endowed a level of stretchability to the semiconducting pathways facilitating exceptional electrical performance under deformation.

This work not only demonstrates a general strategy for controlling film morphology leading to highly stretchable polymeric semiconducting films, but also proposes guidelines for the future

development of highly stretchable optoelectronic devices with high electrical performance characteristics, environmental stability and visual transparency.

4. Associated Content

Experimental details and additional characterization data are described in the Supporting Information. This material is available free of charge via the Internet at http:// pubs.acs.org.

5. Corresponding Author Information

E-mail: ereichmanis@chbe.gatech.edu

6. Notes

The authors declare no competing financial interest.

7. Acknowledgment

The authors appreciate support from the National Science Foundation (DMR 1809495). This work was performed in part at the Georgia Tech Institute for Electronics and Nanotechnology, a member of the National Nanotechnology Coordinated Infrastructure, which is supported by the National Science Foundation (Grant ECCS-1542174). HX thanks the China Scholarship Council. Support from the Georgia Institute of Technology, funds associated with the Pete Silas Chair in Chemical Engineering, the Georgia Tech Center for the Science and Technology of Advanced Materials and Interfaces and the Georgia Tech Polymer Network are also acknowledged.

8. References

(1) Tahk, D., Lee, H. H. and Khang, D.-Y. Elastic Moduli of Organic Electronic Materials by the Buckling Method. *Macromolecules*. **2009**, 42, 7079-7083.
(2) Savagatrup, S., Printz, A. D., Rodriquez, D. and Lipomi, D. J. Best of Both Worlds: Conjugated Polymers Exhibiting Good Photovoltaic Behavior and High Tensile Elasticity. *Macromolecules*. **2014**, 47, 1981-1992.
(3) Root, S. E., Savagatrup, S., Printz, A. D., Rodriquez, D. and Lipomi, D. J. Mechanical Properties of Organic Semiconductors for Stretchable, Highly Flexible, and Mechanically Robust Electronics. *Chemical Reviews*. **2017**, 117, 6467-6499.
(4) Xu, J., Wang, S., Wang, G.-J. N., Zhu, C., Luo, S., Jin, L., Gu, X., Chen, S., Feig, V. R., To, J. W. F., Rondeau-Gagné, S., Park, J., Schroeder, B. C., Lu, C., Oh, J. Y., Wang, Y., Kim, Y.-H., Yan, H., Sinclair, R., Zhou, D., Xue, G., Murmann, B., Linder, C., Cai, W., Tok, J. B.-H., Chung, J. W. and Bao, Z.27-Highly stretchable polymer semiconductor films through the nanoconfinement effect. *Science*. **2017**, 355, 59-64.
(5) Wang, S., Fabiano, S., Himmelberger, S., Puzinas, S., Crispin, X., Salleo, A. and Berggren, M. Experimental evidence that short-range intermolecular aggregation is sufficient for efficient charge transport in conjugated polymers. *Proceedings of the National Academy of Sciences*. **2015**, 112, 10599-10604.
(6) Kang, B., Ge, F., Qiu, L. and Cho, K. Effective Use of Electrically Insulating Units in Organic Semiconductor Thin Films for High-Performance Organic Transistors. *Advanced Electronic Materials*. **2017**, 3, 1600240-n/a.
(7) Wang, S., Oh, J. Y., Xu, J., Tran, H. and Bao, Z. Skin-Inspired Electronics: An Emerging Paradigm. *Accounts of Chemical Research*. **2018**, 51, 1033-1045.

(8) Wang, B., Huang, W., Chi, L., Al-Hashimi, M., Marks, T. J. and Facchetti, A. High-k Gate Dielectrics for Emerging Flexible and Stretchable Electronics. *Chemical Reviews*. **2018**, 118, 5690-5754.
(9) Zhang, G., McBride, M., Persson, N., Lee, S., Dunn, T. J., Toney, M. F., Yuan, Z., Kwon, Y.-H., Chu, P.-H., Risteen, B. and Reichmanis, E. Versatile Interpenetrating Polymer Network Approach to Robust Stretchable Electronic Devices. *Chemistry of Materials*. **2017**, 29, 7645-7652.
(10) Reich, S. and Cohen, Y. Phase separation of polymer blends in thin films. *Journal of Polymer Science: Polymer Physics Edition*. **1981**, 19, 1255-1267.
(11) BATES, F. S. Polymer-Polymer Phase Behavior. *Science*. **1991**, 251, 898-905.
(12) Chua, L. L., Ho, P. K. H., Sirringhaus, H. and Friend, R. H. Observation of Field-Effect Transistor Behavior at Self-Organized Interfaces. *Advanced Materials*. **2004**, 16, 1609-1615.
(13) Kim, J.-S., Ho, P. K. H., Murphy, C. E. and Friend, R. H. Phase Separation in Polyfluorene-Based Conjugated Polymer Blends: Lateral and Vertical Analysis of Blend Spin-Cast Thin Films. *Macromolecules*. **2004**, 37, 2861-2871.
(14) Nilsson, S., Bernasik, A., Budkowski, A. and Moons, E. Morphology and Phase Segregation of Spin-Casted Films of Polyfluorene/PCBM Blends. *Macromolecules*. **2007**, 40, 8291-8301.
(15) Spano, F. C. Modeling disorder in polymer aggregates: The optical spectroscopy of regioregular poly(3-hexylthiophene) thin films. *The Journal of Chemical Physics*. **2005**, 122, 234701.
(16) Pingel, P., Zen, A., Abellón, R. D., Grozema, F. C., Siebbeles, L. D. A. and Neher, D. Temperature-Resolved Local and Macroscopic Charge Carrier Transport in Thin P3HT Layers. *Advanced Functional Materials*. **2010**, 20, 2286-2295.
(17) Chu, P.-H., Kleinhenz, N., Persson, N., McBride, M., Hernandez, J. L., Fu, B., Zhang, G. and Reichmanis, E. Toward Precision Control of Nanofiber Orientation in Conjugated Polymer Thin Films: Impact on Charge Transport. *Chemistry of Materials*. **2016**, 28, 9099-9109.
(18) Yu, W., Zhou, J. and Bragg, A. E. Exciton Conformational Dynamics of Poly(3-hexylthiophene) (P3HT) in Solution from Time-Resolved Resonant-Raman Spectroscopy. *The Journal of Physical Chemistry Letters*. **2012**, 3, 1321-1328.
(19) Yamagata, H. and Spano, F. C. Interplay between intrachain and interchain interactions in semiconducting polymer assemblies: The HJ-aggregate model. *The Journal of Chemical Physics*. **2012**, 136, 184901.
(20) Paquin, F., Yamagata, H., Hestand, N. J., Sakowicz, M., Bérubé, N., Côté, M., Reynolds, L. X., Haque, S. A., Stingelin, N., Spano, F. C. and Silva, C. Two-dimensional spatial coherence of excitons in semicrystalline polymeric semiconductors: Effect of molecular weight. *Physical Review B*. **2013**, 88, 155202.
(21) Spano, F. C. and Silva, C. H- and J-Aggregate Behavior in Polymeric Semiconductors. *Annual Review of Physical Chemistry*. **2014**, 65, 477-500.
(22) Spano, F. C. Modeling disorder in polymer aggregates: The optical spectroscopy of regioregular poly(3-hexylthiophene) thin films. *The Journal of Chemical Physics*. **2005**, 122, 234701.
(23) Hellmann, C., Paquin, F., Treat, N. D., Bruno, A., Reynolds, L. X., Haque, S. A., Stavrinou, P. N., Silva, C. and Stingelin, N. Controlling the Interaction of Light with Polymer Semiconductors. *Advanced Materials*. **2013**, 25, 4906-4911.
(24) Köhler, A., Hoffmann, S. T. and Bässler, H. An Order-Disorder Transition in the Conjugated Polymer MEH-PPV. *Journal of the American Chemical Society*. **2012**, 134, 11594-11601.

(25) Niles, E. T., Roehling, J. D., Yamagata, H., Wise, A. J., Spano, F. C., Moulé, A. J. and Grey, J. K. J-Aggregate Behavior in Poly-3-hexylthiophene Nanofibers. *The Journal of Physical Chemistry Letters*. **2012**, 3, 259-263.
(26) Spano, F. C., Clark, J., Silva, C. and Friend, R. H. Determining exciton coherence from the photoluminescence spectral line shape in poly(3-hexylthiophene) thin films. *The Journal of Chemical Physics*. **2009**, 130, 074904.
(27) Xue, L., Zhang, J. and Han, Y. Phase separation induced ordered patterns in thin polymer blend films. *Progress in Polymer Science*. **2012**, 37, 564-594.
(28) Zhao, K., Wodo, O., Ren, D., Khan, H. U., Niazi, M. R., Hu, H., Abdelsamie, M., Li, R., Li, E. Q., Yu, L., Yan, B., Payne, M. M., Smith, J., Anthony, J. E., Anthopoulos, T. D., Thoroddsen, S. T., Ganapathysubramanian, B. and Amassian, A. Vertical Phase Separation in Small Molecule:Polymer Blend Organic Thin Film Transistors Can Be Dynamically Controlled. *Advanced Functional Materials*. **2016**, 26, 1737-1746.
(29) van Breemen, A., Zaba, T., Khikhlovskyi, V., Michels, J., Janssen, R., Kemerink, M. and Gelinck, G. Surface Directed Phase Separation of Semiconductor Ferroelectric Polymer Blends and their Use in Non-Volatile Memories. *Advanced Functional Materials*. **2015**, 25, 278-286.
(30) Hellmann, C., Treat, N. D., Scaccabarozzi, A. D., Razzell Hollis, J., Fleischli, F. D., Bannock, J. H., de Mello, J., Michels, J. J., Kim, J.-S. and Stingelin, N. Solution processing of polymer semiconductor: Insulator blends-Tailored optical properties through liquid–liquid phase separation control. *Journal of Polymer Science Part B: Polymer Physics*. **2015**, 53, 304-310.
(31) Sharenko, A., Kuik, M., Toney, M. F. and Nguyen, T.-Q. Crystallization-Induced Phase Separation in Solution-Processed Small Molecule Bulk Heterojunction Organic Solar Cells. *Advanced Functional Materials*. **2014**, 24, 3543-3550.
(32) Duong, D. T., Toney, M. F. and Salleo, A. Role of confinement and aggregation in charge transport in semicrystalline polythiophene thin films. *Physical Review B*. **2012**, 86, 205205.
(33) Sirringhaus, H., Brown, P. J., Friend, R. H., Nielsen, M. M., Bechgaard, K., Langeveld-Voss, B. M. W., Spiering, A. J. H., Janssen, R. A. J., Meijer, E. W., Herwig, P. and de Leeuw, D. M. Two-dimensional charge transport in self-organized, high-mobility conjugated polymers. *Nature*. **1999**, 401, 685.
(34) Goffri, S., Muller, C., Stingelin-Stutzmann, N., Breiby, D. W., Radano, C. P., Andreasen, J. W., Thompson, R., Janssen, R. A. J., Nielsen, M. M., Smith, P. and Sirringhaus, H. Multicomponent semiconducting polymer systems with low crystallization-induced percolation threshold. *Nat Mater*. **2006**, 5, 950-956.
(35) Prosa, T. J., Moulton, J., Heeger, A. J. and Winokur, M. J. Diffraction Line-Shape Analysis of Poly(3-dodecylthiophene): A Study of Layer Disorder through the Liquid Crystalline Polymer Transition. *Macromolecules*. **1999**, 32, 4000-4009.
(36) Chang, M., Choi, D., Wang, G., Kleinhenz, N., Persson, N., Park, B. and Reichmanis, E. Photoinduced Anisotropic Assembly of Conjugated Polymers in Insulating Polymer Blends. *ACS Applied Materials & Interfaces*. **2015**, 7, 14095-14103.
(37) Heriot, S. Y. and Jones, R. A. L.37-An interfacial instability in a transient wetting layer leads to lateral phase separation in thin spin-cast polymer-blend films. *Nature Materials*. **2005**, 4, 782.
(38) Tanaka, K., Yoon, J.-S., Takahara, A. and Kajiyama, T. Ultrathinning-Induced Surface Phase Separation of Polystyrene/Poly(vinyl methyl ether) Blend Film. *Macromolecules*. **1995**, 28, 934-938.

TOC:

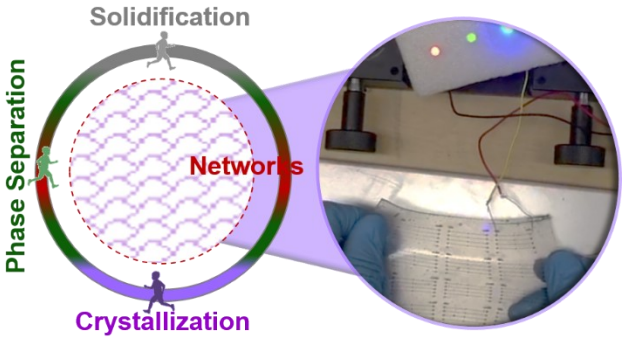
Solidification
Phase Separation
Networks
Crystallization